Sampling and Exploration Strategies for Multi-Agent Seismic Imaging Using 3D Full Waveform Inversion

Ban-Sok Shin and Dmitriy Shutin
Institute of Communications and Navigation, German Aerospace Center
E-Mail: {ban-sok.shin, dmitriy.shutin}@dlr.de

***Abstract*—For future planetary missions, we envision the use of multi-agent networks that autonomously and cooperatively explore a planet's subsurface. To this end, we consider seismic imaging techniques such as full waveform inversion to obtain tomographic images of the subsurface. However, seismic imaging techniques have not been largely investigated yet within the context of robotic exploration. Therefore, in this work we investigate full waveform inversion for subsurface exploration by a multi-agent network. To this end, we assume a small robotic network where each agent is equipped with a geophone. The network shall perform 3D imaging based on measurements recorded over the subsurface of interest. We investigate different sampling and exploration strategies to explore a synthetic subsurface model and evaluate the strategies with respect to their resulting imaging performance. Based on 3D numerical simulations we show that a topology with random agent positions obtains better imaging performance compared to a uniform grid formation. Furthermore, separating the exploration area into smaller areas that overlap with each other gives further performance gains. Our work provides insights in how full waveform inversion can be employed for subsurface exploration by a multi-agent network.**

I. Introduction

Subsurface imaging and exploration is playing an increasing role in planetary missions as can be seen from the InSIGHT or Mars2020 missions [1], [2], [3]. Furthermore, several research projects are dealing with seismic techniques for exploration of caves, lava tubes or icy rocks on Moon, Mars and other planets. For instance, in the ROBEX (Robotic Exploration of Extreme Environments) project robots were used to place seismometers at predefined locations to record seismic measurements [4], [5]. Concepts were demonstrated on analogue sites such as Mt. Etna where the subsurface properties are similar to the Moon. Within NASA JPL's CADRE (Cooperative Autonomous Distributed Robotic Exploration) project a small network of rovers shall conduct cooperative exploration on the Moon using ground penetrating radar [6], [7]. Moreover, the startup IMENSUS deals with resource exploration on the Moon using an autonomous rover that places geophones over the exploration area [8]. In our project NEPOS (Near-Surface Seismic Exploration of Planetary Bodies with Adaptive Networks) we investigate near-surface imaging of caves such as lava tubes that might serve as safe habitats for space equipment, measurement tools or even humans. To this end, a robotic swarm carrying geophones is considered that shall adapt its topology depending on the subsurface under survey [9], [10].

Many of the above mentioned research and development activities intend to use multiple rovers that are equipped with seismic receivers and act autonomously and cooperatively to image the subsurface. In this respect, we proposed several works on distributed seismic tomography where imaging techniques such as traveltime tomography or full waveform inversion are adapted for operation within a network of agents [11], [12]. Here, each agent obtains a global subsurface image locally by data exchange with other agents in the network. Yet seismic exploration and imaging conducted by a robotic swam has not been addressed thoroughly in the literature. One research question in this respect is the optimal placement of rovers/seismic receivers and the employed exploration strategy to image the subsurface with low effort and satisfying accuracy. Regarding optimal seismic surveys several methods have been proposed in [13], [14] based on optimal experimental design. However, these works focus on either seismic source localization or on optimal placement of sources.

In this work, we intend to shed light on the question of how to explore a subsurface in a consecutive fashion by a multi-agent network. To this end, we apply full waveform inversion to a mobile subsurface exploration scenario. Here, a large exploration area is separated into smaller areas and within each area we employ a small multi-agent network that performs seismic measurements and imaging using full waveform inversion (FWI). We investigate how factors such as sampling topology and separation of the exploration area impact FWI in such an exploration scenario. To this end, we perform 3D numerical simulations using randomized and uniform grid sampling for the agent positions. We show empirically that random sampling positions benefit the imaging performance of FWI for exploration. Furthermore, we compare two different strategies to separate the complete exploration area. One strategy considers overlapping exploration areas whereas the second strategy uses non-overlapping areas. Here, we observe that overlapping areas improve the imaging performance of the exploration survey. In our work, we demonstrate that FWI can be successfully applied to multi-agent exploration of subsurfaces.

II. Subsurface Exploration Method

In the following section, we first give a brief review of FWI. After that, we describe how we apply FWI to subsurface exploration conducted by a multi-agent network.

A. Brief review of full waveform inversion

FWI is a seismic imaging technique that recovers subsurface images with respect to material parameters such as wave speed or density [15]. In its original form it is posed as an optimization of an ℓ_2 functional that measures the distance between synthesized seismic data $\boldsymbol{d}_{\text{syn}}(\boldsymbol{m})$ and seismic measurements $\boldsymbol{d}_{\text{obs}}$ recorded at N_{R} receivers:

$$\min_{\boldsymbol{m}} \mathcal{L}(\boldsymbol{m}) = \frac{1}{2}||\boldsymbol{d}_{\text{obs}} - \boldsymbol{d}_{\text{syn}}(\boldsymbol{m})||_2^2. \tag{1}$$

The vector $\boldsymbol{d}_{\text{obs}} \in \mathbb{R}^{N_{\text{T}} N_{\text{R}}}$ is a stacked quantity containing the recorded time series of N_{T} samples of all N_{R} receivers. Vector $\boldsymbol{d}_{\text{syn}}(\boldsymbol{m})$ follows the same structure and has the same dimension. Variable $\boldsymbol{m} \in \mathbb{R}^{N_x N_y N_z}$ is a vectorized estimate of the 3D subsurface with N_x, N_y, N_z being the number of grid cells in x, y, z dimension.

The optimization problem (1) is subjected to side constraints that in case of FWI for P-waves are specified in terms of the acoustic wave equation:

$$\frac{1}{\boldsymbol{m}(\boldsymbol{x})^2} \frac{\partial^2 \boldsymbol{u}(\boldsymbol{x}, t)}{\partial t^2} - \frac{\partial^2 \boldsymbol{u}(\boldsymbol{x}, t)}{\partial \boldsymbol{x}^2} = \boldsymbol{f}(\boldsymbol{x}, t). \tag{2}$$

The wave equation (2) is solved w.r.t. the wavefield $\boldsymbol{u}(\boldsymbol{x}, t)$ that depends on spatial coordinate $\boldsymbol{x}$ and time t. The subsurface model $\boldsymbol{m}(\boldsymbol{x})$ describes the P-wave velocity over space and $\boldsymbol{f}(\boldsymbol{x}, t)$ is a seismic source such as an explosive or hammer strike. To compute $\boldsymbol{d}_{\text{syn}}(\boldsymbol{m})$ the wavefield $\boldsymbol{u}(\boldsymbol{x}, t)$ is sampled at the receiver positions $\boldsymbol{x}_r, r = 1, \ldots, N_{\text{R}}$.

Since problem (1) needs to be solved while satisfying the wave equation (2) it is an optimization problem constrained by a partial differential equation (PDE). Moreover, it is nonlinear in $\boldsymbol{m}(\boldsymbol{x})$, which in general requires application of numerical optimization techniques, such as gradient-based methods. However, computation of the gradient w.r.t the model parameters is not straightforward. For such optimization problems the *adjoint state method* can be used to compute $\nabla_{\boldsymbol{m}} \mathcal{L}(\boldsymbol{m})$ [16]. Then an iterative minimization scheme such as gradient descent can be employed to update the subsurface model via

$$\boldsymbol{m} \leftarrow \boldsymbol{m} - \alpha \nabla_{\boldsymbol{m}} \mathcal{L}(\boldsymbol{m}) \tag{3}$$

where $\alpha > 0$ is a suitable step size. In general, other numerical optimization schemes such as Quasi-Newton methods can be used as well. However, due to the PDE-constraint in problem (1) the cost functional $\mathcal{L}(\boldsymbol{m})$ is highly non-convex with multiple local minima. Hence, to converge to a solution close to the global optimum accurate initialization of FWI is important. For better convergence behavior, the step size has to be adapted accordingly e.g. by a line search.

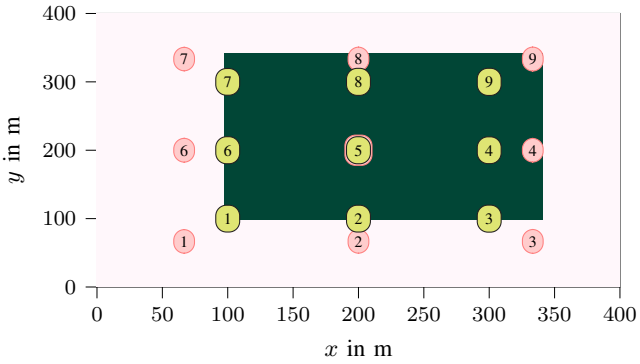

Fig. 1: Center points of exploration areas for **overlapping** and **non-overlapping** strategy. In the background the subsurface model of one cubic anomaly is depicted.

B. Full waveform inversion for exploration

In the following, we investigate the use of FWI for subsurface exploration by a multi-agent network with N_{R} agents. Each agent is equipped with a geophone and measures seismic data at its current position. We assume that at least one agent is connected to all other agents in the network such that all seismic measurements can be processed centrally by FWI. Here, we focus on the generic capability and suitability of FWI to be performed in a sequential manner for a robotic exploration. Therefore, we do not consider distributed processing of the seismic data. Yet we developed corresponding algorithms in [17], [11]. Since the multi-agent network consists of a small number of agents it is limited in its examineable exploration area. Hence, consecutive exploration, where the agents move from one area to another, is required to cover the complete surface of interest. We assume that multiple seismic sources are spread over the exploration area but are fixed in their position.

To perform robotic subsurface exploration using FWI we separate the complete exploration area into smaller exploration domains. In each domain i the agents take measurements and perform FWI to obtain the whole subsurface model $\boldsymbol{m}_i$. Then the agents move to the next domain $i+1$ and repeat the process. To perform FWI in the next domain $i+1$, it is initialized with the estimated subsurface model $\boldsymbol{m}_i$ computed at the previous exploration domain i. Note that we do not accumulate the measurements taken over the course of exploration but instead rely on the reconstructed subsurface model from the previous exploration domain. Hence, in each exploration domain we solve a small, local FWI problem to converge to a global subsurface estimate over the course of exploration.

Two exploration strategies are considered in this work. In the first case, the complete area is separated into equally sized exploration domains that overlap with each other. This is done in order exploit redundancy in the observed data that possibly enhances the imaging performance. As comparison we investigate exploration domains that do not overlap with each other. With respect to the sampling positions of the agents

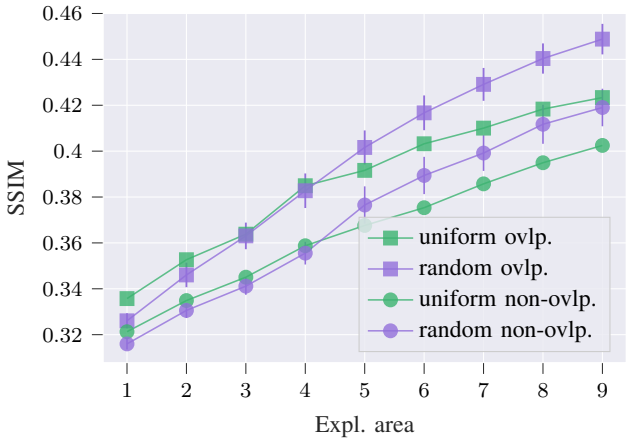

Fig. 2: SSIM for subsurface with one cubic anomaly.

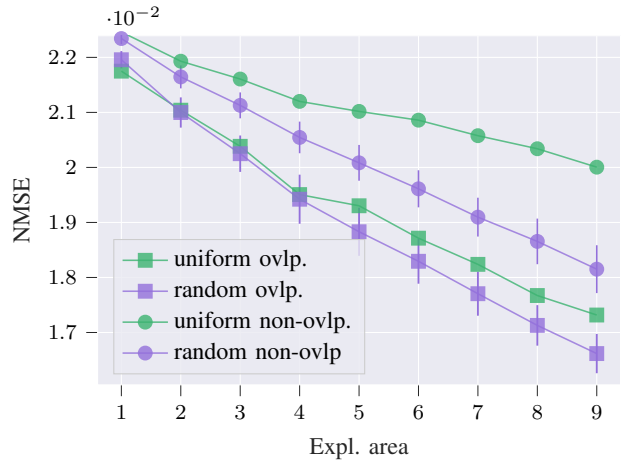

Fig. 3: NMSE for subsurface with one cubic anomaly.

we investigate again two cases. One case considers a uniform grid constellation of the agents in the respective exploration domain. In the second case we consider a random constellation of the agents based on a uniform distribution. The uniform grid is motivated by traditional seismic exploration surveys where the geophones are placed in a uniform grid pattern. Random sampling is motivated by the fact that in realistic exploration scenarios, communication constraints between agents and challenging terrains make setting up a uniform grid difficult. As a result, sampling topologies resulkting from a random topology of the underlying agent's communication network are more likely.

III. Simulation Results

Based on the exploration and sampling strategies introduced in the previous section we conduct 3D numerical simulations with FWI to investigate their performance. We assume a computational domain of $x = 400\,\mathrm{m}, y = 400\,\mathrm{m}, z = 200\,\mathrm{m}$. The domain is discretized by cells of width $\Delta x = \Delta y = \Delta z = 10\,\mathrm{m}$ resulting in $41 \times 41 \times 21$ grid cells in total. We set the number of agents to $N_\mathrm{R} = 9$ and the number of sources to $N_\mathrm{S} = 9$ as well. The sources are spread in a regular 3×3 grid pattern over the complete exploration area and released once the agents reach a new exploration domain.

The complete exploration area is separated into nine smaller exploration domains. In the overlapping strategy each exploration domain has a size of $200\,\mathrm{m} \times 200\,\mathrm{m}$ and half of each domain is overlapping with the preceding one. In the non-overlapping strategy each exploration domain has a size of $133.33\,\mathrm{m} \times 133.33\,\mathrm{m}$ resulting in nine distinct domains.

Regarding the subsurface we consider two synthetic models. The first model contains a cubic anomaly with a constant background velocity. The second model contains two cubic anomalies with a velocity gradient in the background. In both cases, we use blurred versions of the ground truth model as starting model for FWI in the first exploration domain. As performance measures we investigate the normalized mean square error (NMSE) and the structural similarity index measure (SSIM) [18] between reconstructed and true subsurface model.

A. Single cuboid anomaly

We consider a cubic anomaly with a velocity of $2.5\,\mathrm{km\,s^{-1}}$ that is placed inside a domain of constant velocity $2\,\mathrm{km\,s^{-1}}$. Within each exploration domain FWI is performed for $N_\mathrm{FWI} = 10$ iterations. The step size is selected as $\alpha = 0.1$ and is gradually decreased using an exponential decay over the iterations. By that we obtain a gradual decrease of the cost function in each exploration domain. The reconstructed subsurface of one exploration domain is then used as initial model for FWI in the next exploration domain. In the case of random sampling positions we perform 100 Monte Carlo runs with new receiver positions drawn from a uniform distribution per trial. Figure 1 shows the respective center coordinates of the exploration domains for the overlapping and non-overlapping strategy.

Figures 2 and 3 show the resulting SSIM and NMSE, respectively, over the exploration domains. Furthermore, we compare random and uniform sampling positions as well as the strategies of overlapping and non-overlapping exploration domains. First of all, it is visible that both SSIM and NMSE are improving over the exploration domains. Hence, applying FWI consecutively within a small receiver network is possible to explore larger subsurface domains. Furthermore, it is clearly visible that random sampling positions lead to better imaging performance especially in later exploration domains. Moreover, the standard deviation in the SSIM and NMSE for random sampling positions is fairly small showing that such sampling strategy should outperform uniform grids in sequential exploration surveys. Regarding the exploration domains it is noticeable that overlapping domains benefit the imaging performance. This might be due to the fact that overlapping domains support FWI in achieving a more robust convergence behavior since some redundancy in the measurement data is present. Another reason can also be the larger surface area compared to the non-overlapping strategy where each

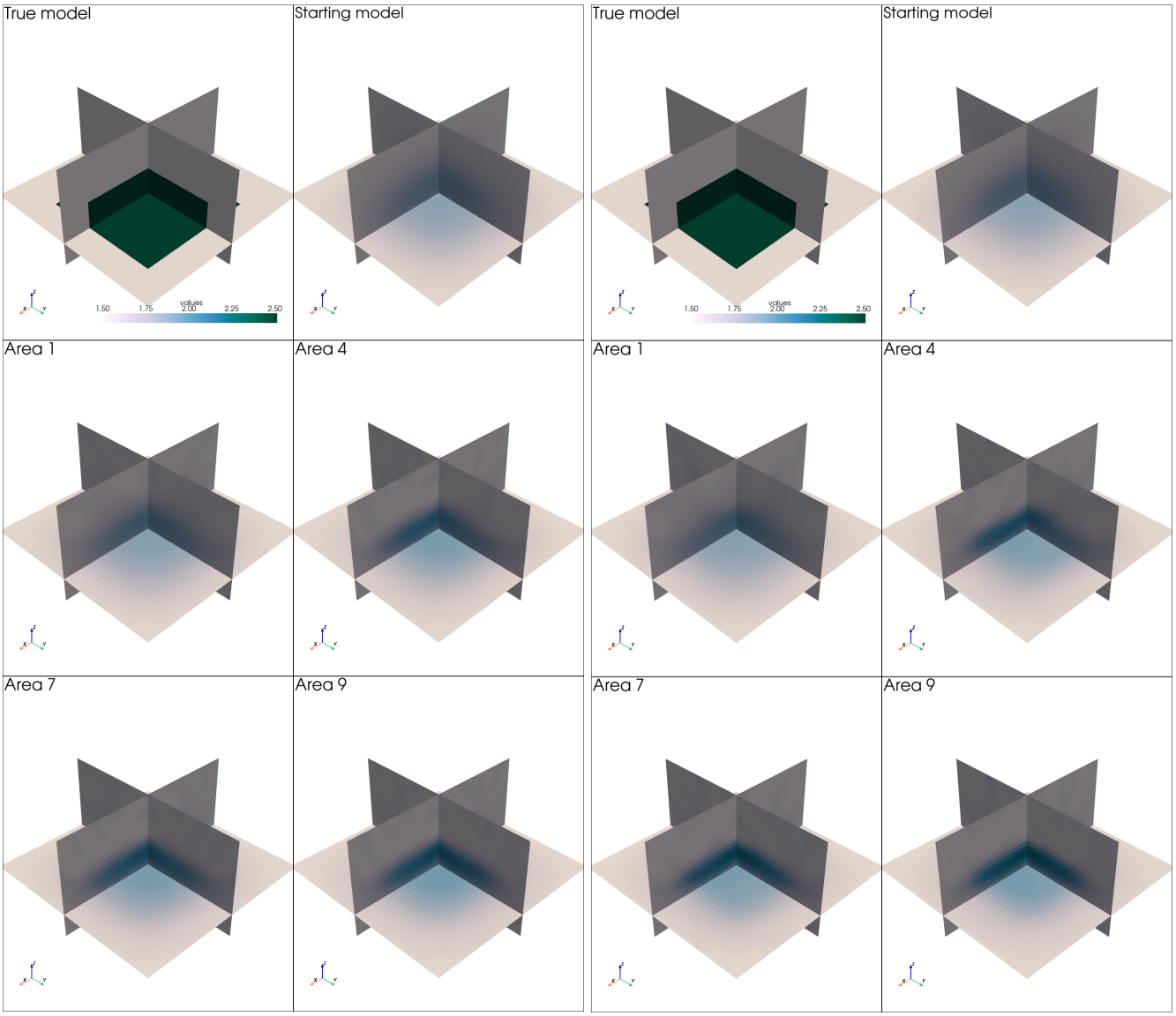

(a) **Uniform grid** in each exploration domain.

(b) **Random** constellation in each exploration domain.

Fig. 4: Recovered 3D subsurface images for subsurface with one cubic anomaly with overlapping exploration domains.

exploration domain is distinct and therefore smaller compared to the overlapping case.

Figures 4a and 4b show examples of the 3D images obtained by FWI exploration using either random or uniform grid sampling positions. One can observe how the reconstruction is improved over the course of exploration areas. In particular, in the last area 9 random sampling results in sharper edges and a more accurate velocity estimate within the anomaly compared to the uniform grid.

B. Two distinct cuboid anomalies with varying background velocity

As a second example we consider two cubic anomalies with velocities $m_1 = 2.3\,\mathrm{m\,s^{-1}}$ and $m_2 = 2.7\,\mathrm{m\,s^{-1}}$, respectively. The background velocity is increased linearly from $1.5\,\mathrm{km\,s^{-1}}$ until $2\,\mathrm{km\,s^{-1}}$. Again, as starting model we assume a blurred version of the ground truth model, as can be seen in Figure 8a.

Figure 6 and 7 show the SSIM and NMSE, respectively, over the exploration areas for both exploration strategies and sampling strategies. As before, random sampling and overlapping exploration areas give the best imaging performance. Compared to a single anomaly one can observe an even higher performance gain that is achieved by random sampling positions. One reason can be that the gain of random sampling becomes more apparent here due to the higher complexity of the subsurface. Both SSIM and NMSE curves of uniform grid sampling flatten out quite quickly compared to the random case. In particular, when investigating the SSIM curve one notices high performance gains from area 3 to 4 and from 8 to 9. From Figure 5 we can see that in area 4 large parts

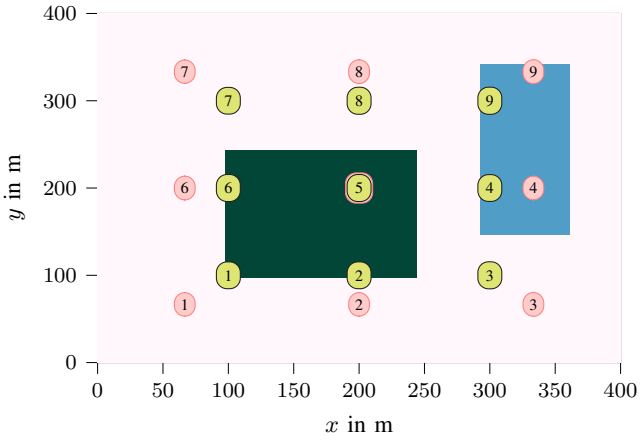

Fig. 5: Center points of exploration domains for **overlapping** and **non-overlapping** strategy. In the background the subsurface model of two cubic anomalies is depicted.

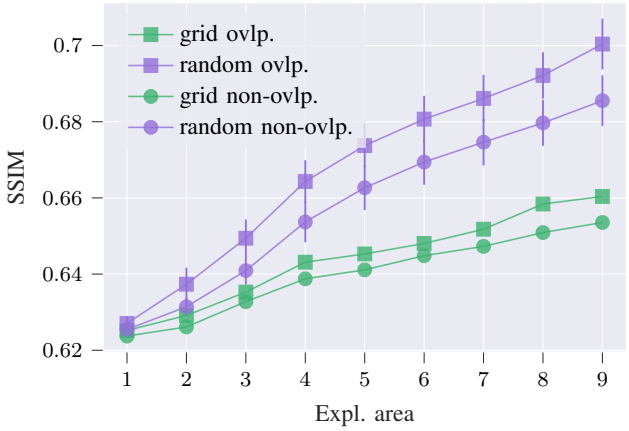

Fig. 6: SSIM for subsurface with two anomalies.

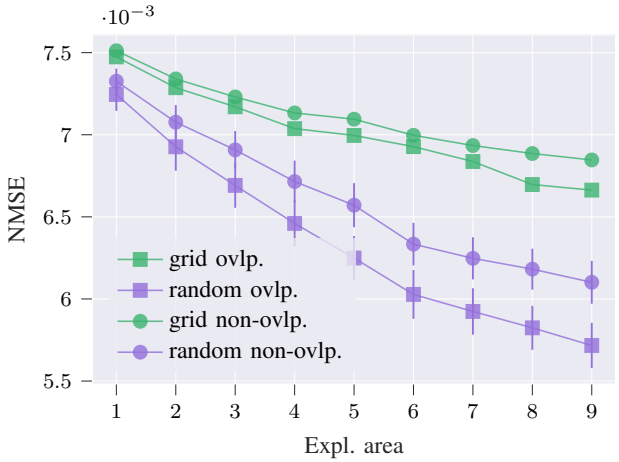

Fig. 7: NMSE for subsurface with two anomalies.

of the vertically shaped anomaly are covered by the agents. Hence, a high performance gain can be observed in the SSIM. The same is true for area 9. For the case of such a more complex subsurface model, random sampling positions result in an even higher performance gain for consecutive exploration using FWI.

Figure 8a and 8b depict two examples of 3D images obtained by uniform grid and random sampling, respectively, over the different exploration areas. Again, random sampling positions benefit the overall imaging performance. Especially, in the last area 9 the thin cubic anomaly is more visible compared to the uniform grid case, where it is barely visible. Since in area 9 covers mostly parts of the thin anomaly, it is better imaged at this stage than before. Furthermore, in random sampling the contour of the larger anomaly is more pronounced with the absolute velocity values closer to the ground truth.

IV. Conclusion

In this paper, we empirically investigated the use of full waveform inversion for subsurface exploration tasks conducted by a multi-agent network. In particular, we compared two sampling topologies with each other: Uniform grid and random positions for the agents. Based on 3D numerical simulations with two different synthetic subsurface models we show that random sampling positions benefit the imaging performance of FWI for a consecutive execution in exploration. Moreover, separating the complete exploration area into small areas that overlap with each other leads to further performance gains. Based on these findings we conclude that it is not necessary to have a uniform grid constellation for FWI for a consecutive exploration. Sampling positions may be chosen rather randomly or depending on terrain and communication conditions among the agents.

For future work, distributed imaging methods such as the adapt-then-combine FWI [11] shall be investigated for operation in such multi-agent exploration scenarios. Such method allows for a completely distributed operation of the imaging procedure and therefore, do not require a central entity, as we have assumed in this work.

V. Acknowledgement

The work leading to this publication was partially funded by the German Research Foundation (DFG) under grant 517291159.

References

[1] B. Fernando, N. Wójcicka, M. Froment *et al.*, "Listening for the landing: Seismic detections of perseverance's arrival at mars with insight," *Earth and Space Science*, vol. 8, no. 4, Apr. 2021.

[2] B. Fernando, N. Wójcicka, R. Maguire, S. C. Stähler *et al.*, "Seismic constraints from a mars impact experiment using insight and perseverance," *Nature Astronomy*, vol. 6, no. 1, p. 59–64, Oct. 2021.

[3] P. Lognonné, W. B. Banerdt, D. Giardini *et al.*, "Seis: Insight's seismic experiment for internal structure of mars," *Space Science Reviews*, vol. 215, no. 1, Jan. 2019. [Online]. Available: http://dx.doi.org/10.1007/s11214-018-0574-6

[4] A. Wedler, M. Hellerer, B. Rebele, H. Gmeiner *et al.*, "Robex – components and methods for the planetary exploration demonstration mission," in *13th Symposium on Advanced Space Technologies in Robotics and Automation (ASTRA)*, ser. ASTRA, 2015.

[5] "Robotic exploration of extreme environments (ROBEX)," https://www.imensusresources.com/solutions/seismic-exploration-rover/, 2024, [Accessed 29-07-2024].

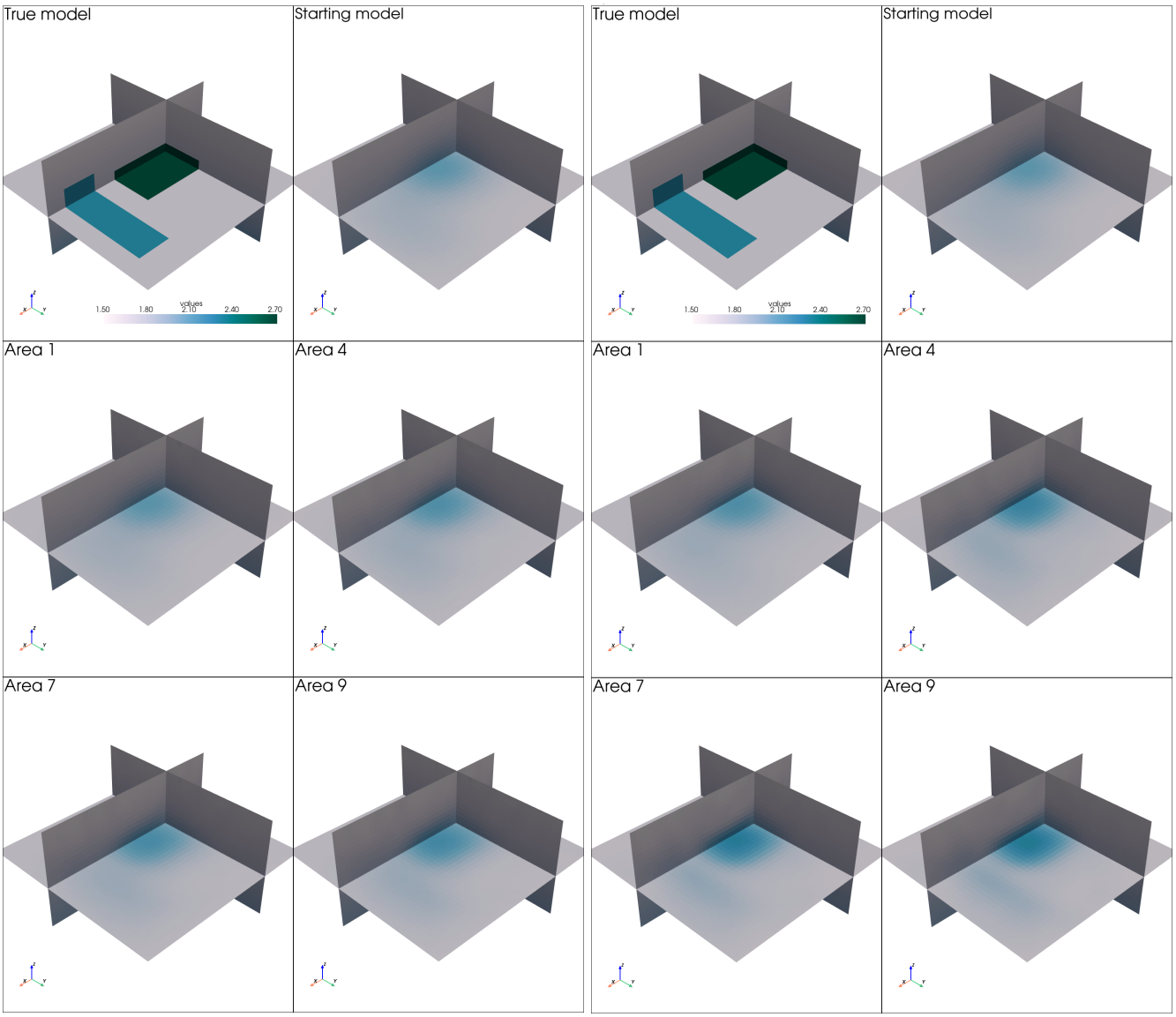

(a) **Uniform grid** in each exploration area.

(b) **Random** constellation in each exploration area.

Fig. 8: Recovered 3D subsurface images for subsurface with two cubic anomalies with overlapping exploration areas.

[6] J.-P. de la Croix, F. Rossi, R. Brockers, D. Aguilar *et al.*, "Multi-agent autonomy for space exploration on the cadre lunar technology demonstration," in *2024 IEEE Aerospace Conference*, 2024, pp. 1–14.

[7] "NASA JPL - cooperative autonomous distributed robotic exploration (CADRE)," https://www.nasa.gov/cooperative-autonomous-distributed-robotic-exploration-cadre/, 2024, [Accessed 29-07-2024].

[8] "Seismic exploration rover - imensusresources.com," https://www.imensusresources.com/solutions/seismic-exploration-rover/, 2024, [Accessed 29-07-2024].

[9] S. Keil, H. Igel, F. Bernauer *et al.*, "The NEPOS Project: Near-Surface Seismic Exploration of Planetary Bodies with Adaptive Networks," in *AGU Fall Meeting Abstracts*, vol. 2023, Dec. 2023, pp. P11C–2746.

[10] K. Nierula, D. Shutin, B.-S. Shin *et al.*, "Probabilistic approach toward seismic exploration with autonomous robotic swarms," in *EGU General Assembly 2024*, April 2024.

[11] B.-S. Shin and D. Shutin, "Joint distributed traveltime and full waveform tomography for enhanced subsurface imaging in seismic networks," *IEEE Trans. Comput. Imaging*, vol. 10, p. 600–612, 2024.

[12] B.-S. Shin, D. Patel, L. Wientgens, D. Shutin, and A. Dekorsy, "Multi-agent 3d seismic exploration using adapt-then-combine full waveform inversion in a hardware-in-the-loop system," in *IEEE International Conference on Acoustics, Speech and Signal Processing*, Apr. 2024.

[13] V. Krampe, P. Edme, and H. Maurer, "Optimized experimental design for seismic full waveform inversion: A computationally efficient method including a flexible implementation of acquisition costs," *Geophysical Prospecting*, vol. 69, no. 1, p. 152–166, Oct. 2020.

[14] D. Strutz and A. Curtis, "Variational bayesian experimental design for geophysical applications: seismic source location, amplitude versus offset inversion, and estimating co2 saturations in a subsurface reservoir," *Geophys. J. Int.*, vol. 236, no. 3, p. 1309–1331, 2023.

[15] J. Virieux and S. Operto, "An overview of full-waveform inversion in exploration geophysics," *Geophysics*, vol. 74, no. 6, 2009.

[16] R. E. Plessix, "A review of the adjoint-state method for computing the gradient of a functional with geophysical applications," *Geophys. J. Int.*, vol. 167, no. 2, pp. 495–503, 2006.

[17] B.-S. Shin and D. Shutin, "Distributed traveltime tomography using kernel-based regression in seismic networks," *IEEE Geoscience and Remote Sensing Letters*, vol. 19, p. 1–5, 2022.

[18] Z. Wang, A. Bovik, H. Sheikh, and E. Simoncelli, "Image quality assessment: From error visibility to structural similarity," *IEEE Transactions on Image Processing*, vol. 13, no. 4, p. 600–612, Apr. 2004.